AGU PUBLICATIONS

Geophysical Research Letters

RESEARCH LETTER
10.1002/2015GL066297

Key Points:
- Rising autocorrelation, a common indicator of abrupt change, can raise false alarms for sea ice
- Changes in effective heat capacity, rather than bifurcations, dominate the autocorrelation signal
- Rising autocorrelation is not a universal indicator for abrupt change in physical systems

Correspondence to:
T. J. W. Wagner,
tjwagner@ucsd.edu

Citation:
Wagner, T. J. W., and I. Eisenman (2015), False alarms: How early warning signals falsely predict abrupt sea ice loss, *Geophys. Res. Lett.*, *42*, doi:10.1002/2015GL066297.

Received 22 SEP 2015
Accepted 16 NOV 2015
Accepted article online 24 NOV 2015

False alarms: How early warning signals falsely predict abrupt sea ice loss

Till J. W. Wagner[1] and Ian Eisenman[1]

[1] Scripps Institution of Oceanography, University of California at San Diego, La Jolla, California, USA

Abstract Uncovering universal early warning signals for critical transitions has become a coveted goal in diverse scientific disciplines, ranging from climate science to financial mathematics. There has been a flurry of recent research proposing such signals, with increasing autocorrelation and increasing variance being among the most widely discussed candidates. A number of studies have suggested that increasing autocorrelation alone may suffice to signal an impending transition, although some others have questioned this. Here we consider variance and autocorrelation in the context of sea ice loss in an idealized model of the global climate system. The model features no bifurcation, nor increased rate of retreat, as the ice disappears. Nonetheless, the autocorrelation of summer sea ice area is found to increase in a global warming scenario. The variance, by contrast, decreases. A simple physical mechanism is proposed to explain the occurrence of increasing autocorrelation but not variance when there is no approaching bifurcation. Additionally, a similar mechanism is shown to allow an increase in both indicators with no physically attainable bifurcation. This implies that relying on autocorrelation and variance as early warning signals can raise false alarms in the climate system, warning of "tipping points" that are not actually there.

1. Introduction

The notion of critical slow down (CSD) as giving rise to "universal" early warning signals (EWS) for critical transitions has received much attention in recent years. The great appeal of such indicators is their system independence: any dynamical system featuring certain critical transitions, such as bifurcations, is expected to undergo CSD as it gradually approaches a transition point, regardless of whether the system is a financial market, an ecosystem, or an aspect of Earth's climate. A generic EWS would ideally warn in advance of an impending catastrophic shift without requiring detailed knowledge of the dynamics of the system. CSD can have a number of measurable effects in observational time series. Two of the most commonly discussed ones are (i) the amplification in stochastic fluctuations around the dynamical equilibrium, which manifests as an increase in variance and (ii) increased autocorrelation, which is related to slower response times to stochastic perturbations. Both increased variance and increased autocorrelation have been considered as potential indicators of approaching a critical transition in numerous studies [*Scheffer et al.*, 2009, 2012]: applications range from predicting short-term stock market returns [*LeBaron*, 1992] to market crashes [*Hong and Stein*, 2003], from simple theoretical ecological models [*Wissel*, 1984] to ecosystem-wide field experiments [*Carpenter and Brock*, 2006], and from paleoproxy time series and idealized climate model results [*Dakos et al.*, 2008; *Held and Kleinen*, 2004; *Kleinen et al.*, 2003; *Lenton et al.*, 2012] to modern-day satellite observations [*Livina and Lenton*, 2013]. A number of studies have suggested that increasing autocorrelation alone may suffice to signal an impending transition [*Dakos et al.*, 2008; *Lenton et al.*, 2012].

However, the exact conditions under which CSD can be deduced from observational time series are disputed in some recent studies [*Boettiger and Hastings*, 2012a, 2012b; *Dakos et al.*, 2012], and it has been suggested that rising autocorrelation alone does not indicate CSD [*Ditlevsen and Johnsen*, 2010]. Furthermore, CSD has been suggested to have limitations as a generic predictor of critical transitions (see review in *Dakos et al.* [2015], occasionally allowing "missed alarms" (not predicting an impending critical transition [*Boettiger and Hastings*, 2013]) as well as "false alarms" (erroneously predicting a critical transition where there is none [*Kefi et al.*, 2013]). These failures can be due to a data set being ill-suited to detect CSD, or they can be a result of conceptually misunderstanding how CSD is linked to the dynamics of a system [*Dakos et al.*, 2015]. Here we are concerned with the latter case.

Among systems that may undergo a bifurcation or "tipping point," Arctic sea ice has been the subject of ardent recent research [e.g., *Winton*, 2006; *Lenton et al.*, 2008; *Notz*, 2009; *Eisenman and Wettlaufer*, 2009; *Lenton*, 2012], and EWS have been considered in this context [*Livina and Lenton*, 2013; S. Bathiany et al., Trends in sea ice variability on the way to an ice-free Arctic, submitted to *The Cryosphere Discussions*, 2015]. The hypothesized tipping point is usually attributed to the ice-albedo feedback, which leads to a loss of stability during sea ice retreat. In a previous paper, we showed that low-order climate models often feature spurious bifurcations which disappear when relevant leading-order physical processes are included [*Wagner and Eisenman*, 2015, hereinafter WE15]. The somewhat more complex climate model introduced in WE15 supports the findings of general circulation models (GCMs), which predict a gradual loss of Arctic sea ice, without crossing a bifurcation, in contrast to many low-order climate models. Here we use the WE15 model to investigate how variance and autocorrelation evolve under global warming.

2. Simulated Sea Ice Loss During Global Warming

The model represents a zonally uniform aquaplanet with a slab ocean mixed layer that includes sea ice. It evolves the seasonally varying surface temperature and sea ice thickness as functions of latitude. The state of the system is given by the surface enthalpy, $E(t,x)$, which contains information about both surface temperature and ice thickness, with time t, $x \equiv \sin\theta$, and latitude θ. Specifically, in ice-covered regions, $E = -L_f h$, with ice thickness h and latent heat of fusion L_f; in ice-free regions, $E = c_w T$. Here c_w is the heat capacity of the ocean mixed layer, and T is the surface temperature measured in terms of the departure from the melting point. We simulate natural variability by adding a weather-like stochastic forcing [*Hasselmann*, 1976] to the deterministic model of WE15. The model can be summarized by a single stochastic partial differential equation:

$$\frac{\partial E}{\partial t} = \underbrace{aS}_{\text{solar}} - \underbrace{(A+BT)}_{\text{OLR}} + \underbrace{D\nabla_x^2 T}_{\text{transport}} + \underbrace{F_b}_{\text{ocean heating}} + \underbrace{F}_{\text{climate forcing}} + \underbrace{N}_{\text{noise}}. \tag{1}$$

The net energy flux on the right-hand side consists of seasonally varying solar radiation, $S(t,x)$, scaled by a coalbedo that depends on the solar zenith angle as well as on the presence of ice, $a(x,E)$; a representation of outgoing longwave radiation (OLR) that is linearized in the surface temperature, $A+BT$, with A and B constants; meridional heat transport in the atmosphere and ocean, represented as diffusion, $D\nabla_x^2 T$; upward heat flux from the ocean below, F_b; climate forcing F, which can be varied to represent changing greenhouse gas levels; and weather noise N, which is stochastic forcing with a persistence timescale of 1 week. Further details of the model formulation are given in Appendix A.

We start the model simulations from a spun-up state with $F = 0$, which corresponds to preindustrial forcing levels and features a perennial ice cover in high latitudes. In order to capture the full dynamic range of the system—from snowball earth to an ice-free pole—we perform an ensemble of realizations for two sets of simulations: (i) warming runs in which F is gradually increased until a perennially ice-free state is reached and (ii) cooling runs in which F is gradually decreased until the planet is completely ice covered. We define A_i as the summer (September) Arctic sea ice area (not to be confused with the constant A). We focus here on A_i, as this quantity typically receives the most widespread attention. Figure 1a shows the evolution of A_i as F is ramped up (red) or down (blue). We compute the variance, σ^2, and lag-1 autocorrelation, ρ, of A_i (see Appendix B for details). The variations of these two indicators with changing forcing F are shown in Figures 1b and 1c.

3. Successful Early Warning For Snowball Earth Bifurcation

The left-hand side of Figure 1a illustrates a bifurcation that is typically found in climate models: the "snowball Earth instability," which is driven by the ice-albedo feedback [e.g., *Pierrehumbert et al.*, 2011]. Starting from a partial ice cover and cooling the model beyond $F = -12$ W m^{-2} leads to an abrupt transition to a fully glaciated Earth (blue curves in Figure 1). Figures 1b and 1c illustrate how both variance and autocorrelation increase as the instability draws near: both EWS indicators accurately give early warning here that the cooling system is approaching a bifurcation.

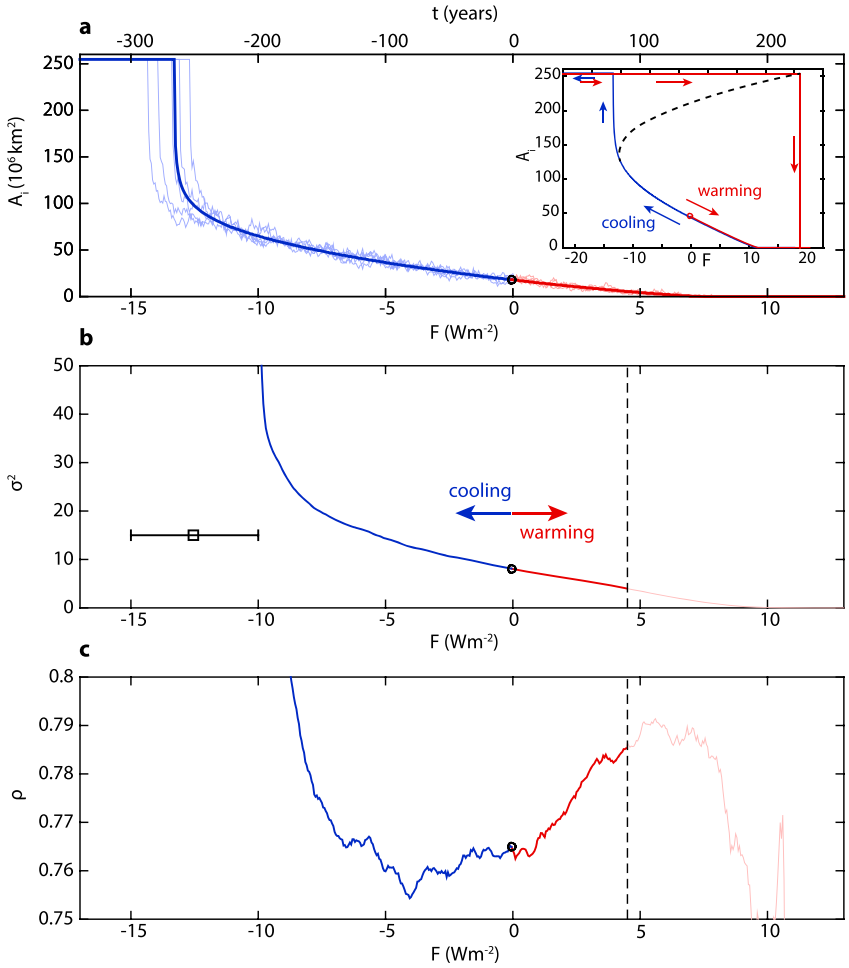

Figure 1. Sea ice area and CSD indicators in a model of global climate and sea ice. (a) Evolution of September Arctic sea ice area A_i, with climate forcing F (lower horizontal axis) and time t (upper horizontal axis). Five realizations of warming and cooling from the 1000-run ensemble are shown (faint red and blue), as well as warming and cooling simulations with no added noise (dark red and blue). Inset: Simulated hysteresis loop of the model with no added noise, with a schematic indication of the unstable state (black dash); arrows indicate warming and cooling trajectories. (b) Variance of the time series in Figure 1a, computed using a 100 year running window (black bar). The variance is plotted above the value of F at the center of the window. The dashed vertical line marks the point where the first realization becomes ice-free in September. (c) As in Figure 1b but for lag-1 autocorrelation. See Appendix B for details. Faint red curves show ρ and σ^2 for running windows that contain values of $A_i = 0$.

4. False Alarm From Rising Autocorrelation

We next consider global warming simulations (red curves in Figure 1), which have steady ice loss until the Arctic becomes icefree in September. The variance decreases monotonically with F over the entire range plotted in Figure 1b. Note that some GCMs simulate an increase in variance of September Arctic sea ice area under global warming, while others simulate a decrease [*Goosse et al.*, 2009]. The autocorrelation in Figure 1c, however, exhibits a marked increase as ice-free conditions are approached.

A rise in autocorrelation alone, without an accompanying rise in variance, is often considered as an EWS of an approaching abrupt transition [e.g., *Dakos et al.*, 2008; *Lenton et al.*, 2012]. Hence, with a limited time series, for example ending at $t = 60$ years ($F = 3$ W m^{-2}), the results in Figure 1c would be interpreted to imply an approaching sudden loss of the remaining sea ice. This would be a false alarm: when F continues to increase, there is no bifurcation nor even an increased rate of retreat as A_i reaches zero (Figure 1a).

Note that the statistical behavior is qualitatively the same when considering winter (March) or annual mean sea ice area (not shown). For March, September, and annual mean sea ice volume, however, both variance

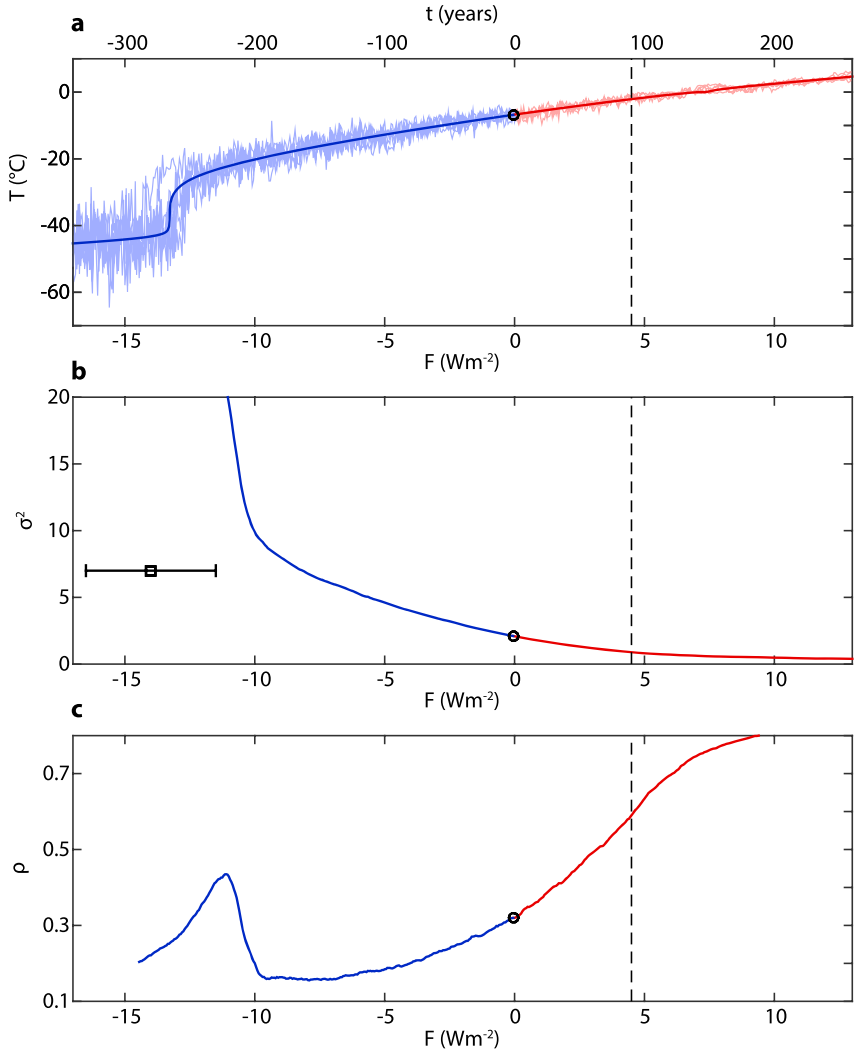

Figure 2. Simulated polar temperature, T_p, and CSD indicators. As in Figure 1 but for September polar temperature instead of ice area.

and autocorrelation decrease monotonically with increasing F. This raises the question whether volume may be a better suited variable than area for assessing the stability of the Arctic sea ice cover. Bathiany et al. (submitted manuscript) consider ice thickness and volume in models that abruptly lose winter ice. They focus on single-column sea ice models which feature a bifurcation associated with this loss, in contrast with the model considered here which has no such bifurcation (see WE15). Consistent with earlier work [*Moon and Wettlaufer*, 2011; *Eisenman*, 2012], the authors find that the response time lengthens in these models before the abrupt winter ice loss. However, they find that this EWS occurs in an impractically narrow range of the parameter space, whereas changes in autocorrelation attributed to physical processes such as those explored here occur in much of the parameter space.

Figure 2 gives the time series of the September temperature at the pole, T_p. It behaves similarly to A_i, with the variance decreasing and the autocorrelation increasing under warming. Since T_p is defined at a single location, this allows for the possibility that spatial variability is not necessary to explain this behavior. We make use of this in the following section.

5. Mechanism For Rising Autocorrelation

What physical mechanism gives rise to the increase in autocorrelation under warming? WE15 found that meridional heat transport and seasonal variations act to essentially remove the effect of nonlinearity from

albedo changes. Hence, the removal of the heat transport term (setting $D = 0$) as well as variations in the solar forcing and albedo from the model (1) may plausibly have compensating effects, leaving the results qualitatively unaffected. With these terms removed, there is no spatial dependence. The influence of sea ice thermodynamic growth (which relates T to E in the model) is still a source of complexity, but with no seasonal cycle, we can crudely approximate this as a change in the effective heat capacity associated with T. This effective heat capacity includes latent heat effects associated with ice melt and growth. Using the WE15 model with $D=0$ and constant aS gives a timescale for the approach to equilibrium, τ, which is 5 times larger for ice-free conditions than for ice. Specifically, $\tau \approx 1$ year for perennial ice near the transition to seasonal ice and $\tau \approx 5$ years for conditions that are ice-free all year; note that these timescales differ somewhat from previous single-column model results [*Moon and Wettlaufer*, 2011; *Eisenman*, 2012, Bathiany et al., submitted manuscript] due to slightly different parameter values and the suppression here of the ice-albedo feedback.

We are then left with the stochastic differential equation:

$$c\frac{dT}{dt} = aS - (A + BT) + F_b + F + N, \tag{2}$$

with a jump in the effective heat capacity c such that $c(T<0)=c_w/5$ and $c(T>0) = c_w$. We take the stochastic forcing, N, to be white noise of intensity σ_1, which is a further simplification compared to the reddened noise used in (1). In this case (2) represents a linear Ornstein-Uhlenbeck process of intensity $\sigma_{OU} = \sigma_1/c(T)$, which recovers from perturbations on a timescale of $\tau = c(T)/B$.

We numerically integrate (2), gradually ramping F such that the equilibrium temperature increases through zero (see Appendix C). The equilibrium value of T varies linearly with the control parameter F, with no bifurcation or accelerated transition occurring as the forcing is increased (Figure 3a). The only nonlinearity is an increase in the effective heat capacity associated with the transition from sea ice to open ocean. The indicators $\sigma^2(T)$ and $\rho(T)$ are computed as in the previous section. Away from the transition at $T = 0$, analytic estimates of variance and autocorrelation are readily calculated. The fluctuation-dissipation theorem implies $\sigma^2(T) = \sigma_{OU}^2\tau/2 = \sigma_1^2/2B^2\tau$, such that the variance decreases when T rises above the freezing point (Figure 3b). Note that for a typical Ornstein-Uhlenbeck process with constant c, $\sigma^2 \propto \tau$, and the inverse relation found here is due to the c dependence of the noise amplitude. The lag-1 autocorrelation with a sampling period of $\Delta t = 1$ year can be shown to be $\rho(T) = \exp(-\Delta t/\tau)$, and hence, it increases when T rises above the freezing point (Figure 3c). The changes in both ρ and σ^2 occur gradually due to the noise causing T to fluctuate above and below 0 for a range of F values.

We consider the September polar temperature T_p in the full model (1) as a point of contact with T in the simplified equation (2). Figure 3 resembles the WE15 model results in Figure 2, suggesting a physical explanation for the mixed EWS behavior: the increase in effective heat capacity when sea ice is replaced with open ocean causes the autocorrelation to increase while the variance decreases.

Hence, in some climate scenarios the autocorrelation increases when there is no approaching bifurcation. A slowdown in variability associated with changes in the relevant heat capacity of the system may also occur in other components of the climate system such as the Pacific Decadal Oscillation [e.g., *Boulton and Lenton*, 2015]. Next, we consider a climate scenario in which both autocorrelation and variance increase without a physically attainable bifurcation.

6. Mechanism For Increase in Both Autocorrelation and Variance

We adjust (2) by allowing for a gradual change in the climate feedbacks, represented by B. For simplicity, here we hold $c = c_w$ constant. As a simple physical example of this, we examine changes in the Planck feedback due to the nonlinearity of the Stefan-Boltzmann relationship, replacing $A + BT$ with $\epsilon\sigma_S\tilde{T}^4$. Here $\tilde{T} \equiv \tilde{T}_m + T$ is the absolute temperature, with melting point $\tilde{T}_m$; σ_S is the Stefan-Boltzmann constant; and we set the effective surface emissivity due to the atmosphere to $\epsilon = A/(\sigma_S\tilde{T}_m^4) = 0.65$. We note that there are many other examples of changing climate feedback strengths, including the ice-albedo feedback. In the resulting system,

$$c_w\frac{d\tilde{T}}{dt} = aS - \epsilon\sigma_S\tilde{T}^4 + F_b + F + N, \tag{3}$$

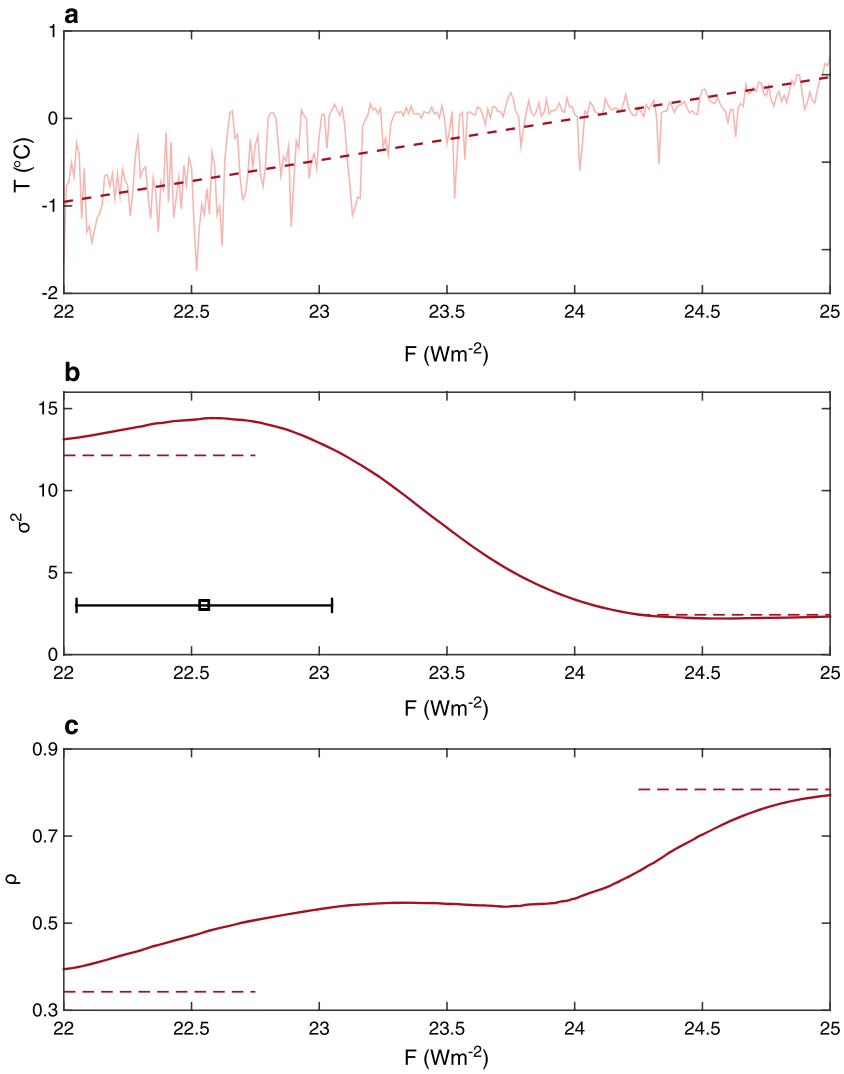

Figure 3. Temperature and CSD indicators for a simple model with a jump in heat capacity. (a) One realization of the stochastic warming simulation (faint red), as well as the noise-free solution (dashed). (b) Variance and (c) autocorrelation, respectively, as in previous figures, with analytic solutions (dashed lines) for $T < 0$ and $T > 0$. Note that the forcing range is shifted compared to previous figures (see Appendix C).

the recovery timescale is approximately $\tau \equiv c_w/(4\epsilon\sigma_S\tilde{T}^3)$, which can be derived by linearizing the system about a given value of $\tilde{T}$. We integrate equation (3) and compute $\sigma^2(\tilde{T})$ and $\rho(\tilde{T})$ as above (see Appendix C). Figure 4 shows that both variance and autocorrelation go up as F decreases and the climate cools.

Interpreted in the context of EWS, these increases raise a false alarm: no abrupt transition will occur as the system (3) cools (although a bifurcation would occur if the system could cool across absolute zero). The state of the system can be seen as located in a single potential well, centered around the equilibrium state set by F. As F decreases, the stabilizing Planck feedback becomes weaker. This leads to a widening of the potential well, causing larger and longer-lasting responses to perturbations.

7. Conclusions

Taken together, the present results imply that using variance and autocorrelation as EWS may raise false alarms during Arctic sea ice retreat, warning of bifurcations that are not actually there. A rise in autocorrelation alone has previously been argued to be a sufficient EWS of an approaching "tipping point" [*Dakos et al.*, 2012; *Lenton et al.*, 2012] or of system acceleration [*Kefi et al.*, 2013]. We instead find that such a rise can occur due to changes in effective heat capacity when there is no acceleration in the sea ice decline. Our result is in agreement with

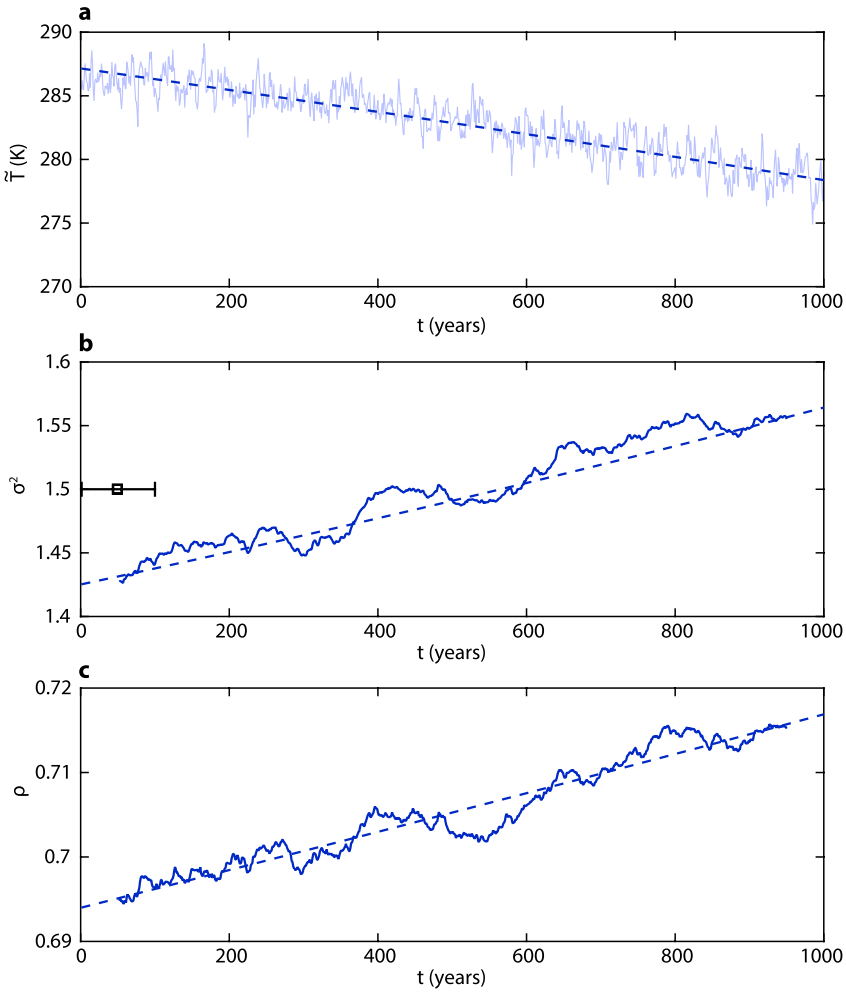

Figure 4. Temperature and CSD indicators for a simple model undergoing cooling with varying Planck feedback. Panels are as in Figure 3, with time *t*, rather than *F*, shown on the horizontal axis; note that here *F* decreases with *t*.

the suggestion that an increase in autocorrelation needs to be accompanied by an increase in variance to function as an EWS [*Ditlevsen and Johnsen*, 2010]. However, we also find that changing climate feedbacks can lead to an increase in both variance and autocorrelation in a system with no physically attainable critical transition. Hence, an increase in one or both of the two indicators is not sufficient to determine the approach of an abrupt transition without knowledge of the underlying dynamics.

Appendix A: Energy Balance-Sea Ice Model

The parameters in the model (1) are set to their default values from WE15, with the exception of *A*, which is set to a value 3 W m^{-2} lower than in WE15. $F = 0$ in the present model then corresponds approximately to preindustrial rather than modern conditions, allowing simulations with increasing *F* to include observed sea ice retreat. Here we ramp *F* up by 15 W m^{-2} over 300 years in the warming simulations and ramp *F* down by 20 W m^{-2} over 400 years in the cooling simulations.

Unlike in WE15, we force the present model with stochastic noise, *N*. The noise at each time step *i* is computed as $N_i = \alpha N_{i-1} + \sqrt{1-\alpha^2}\sigma_0\eta$, with $\sigma_0\eta$ representing a random draw from a Gaussian distribution with mean zero and variance σ_0^2. The noise is slightly reddened with an autocorrelation coefficient of $\alpha \equiv \exp(-\Delta t/\tau_r)$, where the correlation time of $\tau_r = 1$ week is set to be long enough to allow a relatively large Δt. It is further similar to the few-day timescale of observed Arctic surface temperature persistence [e.g., *Walsh et al.*, 2005]. We use $\Delta t = 0.3$ days. To test whether this time step size is sufficiently converged, we compute two 500-member ensembles of 100 year simulations with constant $F = 0$: one ensemble with $\Delta t = 0.03$ days and

one with $\Delta t = 0.3$ days. Considering the time series of A_i in each realization, the difference in the ensemble-mean value of σ^2 between the two ensembles is 0.22; for ρ it is 0.0071. These differences are also partially due to the different realizations of noise in the two ensembles. Both of these are considerably smaller than the signals discussed in Figures 1b and 1c. The noise intensity is chosen such that the resulting Arctic sea ice extent variability is similar to the observations. In addition to the simulations with spatially uniform noise, we considered a smaller ensemble of simulations with spatially varying noise that was set to be autocorrelated in space with a length scale of ~10° latitude. Initial results suggest a similar qualitative result for Figure 1 in both cases, although further work is merited. In the present study, we limit our discussion here to the simpler case of spatially uniform noise.

The simulated ice area is computed as $A_i = \left(1 - x_i\right) A_{\text{hem}}$, where $A_{\text{hem}} = 255 \times 10^6$ km^2 is the surface area of a hemisphere of the earth and x_i is the location of the ice edge. Note that there is very little nonlinear rectification of the noise in this model, which would result in the stochastic ensemble mean deviating noticeably from the deterministic simulation. The stochastic ensemble mean in Figure 1a never deviates from the deterministic simulation by more than $\simeq 1 \times 10^6$ km^2. These deviations visually resemble noise, implying that a larger number of realizations would be needed to construct a sufficiently precise stochastic ensemble mean for these purposes. This finding stands in contrast to previous studies of single-column sea ice models, where there is typically a high level of nonlinear rectification [e.g., *Eisenman*, 2012]. Further details regarding the model described in (1) are given in WE15.

Appendix B: Computation of σ^2 and ρ

All figures are generated using ensembles of 1000 realizations. This ensemble size is chosen to allow sufficient convergence of ρ in model (1). To determine whether ρ is sufficiently converged, we consider the slope of the curve in Figure 1c in the range $F = [-4, 5]$ W m^{-2}. We generate 200 overlapping ensembles that each have 500 realizations by randomly picking sets of 500 runs (with replacement) from the full ensemble of 1000 runs. For each of these 500-member ensembles we generate data such as in Figure 1c and compute the linear trend in the specified range using ordinary least squares regression. We find that 190 of the 200 ensembles have positive trends, which suggests that the rise in ρ would be significant at the 95% level with an ensemble size of 500 and that it is significant above this level with an ensemble size of 1000.

Anomalies are computed by subtracting the ensemble mean from individual runs. For all models, σ^2 and ρ are computed from the anomalies using a running window length of 100 years. The results depend somewhat on the window length. For example, the increase in ρ in Figure 1c is robust for window lengths in the range of roughly 50 to 200 years, and in Figure 2c the increase in ρ is robust down to window lengths of 10 years.

The variance σ^2 is readily computed using the ensemble mean within each window. The computation of the autocorrelation, however, is not as straightforward. To obtain ρ, we compute the correlation between the value at each time within the window in the full ensemble and the value at the previous time. In other words, we generate an array of values at the current time as $X_1 \equiv \left[x_{1,j+1}, \ldots, x_{1,j+L}, \ldots, x_{m,j+1}, \ldots, x_{m,j+L}\right]$, and we also generate an array of values at the previous time as $X_2 \equiv \left[x_{1,j}, \ldots, x_{1,j+L-1}, \ldots, x_{m,j}, \ldots, x_{m,j+L-1}\right]$. Here the first index represents the ensemble member, with $m = 1000$ being the total number of members, and the second index represents time, with the window spanning from time index j to time index $j + L$ (where $L = 100$). The autocorrelation is computed as the correlation between X_1 and X_2.

Appendix C: Integration of Simple Models

In the simpler model (2), the WE15 annual mean polar ice-free values for shortwave radiation are used, $S = 180$ W m^{-2} and $a = 0.6$. Values of c_w, B, and F_b are as in the full model (1). We set the noise amplitude, σ_1, to a value 2 times larger than the full model (1). The OLR is set to $A = 136$ W m^{-2} to compensate for the colder pole due to the lack of horizontal diffusion. The model is integrated over 1000 years with F ramping linearly from 18.5 to 28.5 W m^{-2}, using a time step of $\Delta t = 0.01$ year, and a 1 year sampling period is used in the computation of σ^2 and ρ. Figure 3 shows the 300 year integration period corresponding to $F = [22, 25]$ W m^{-2}. We note that there is an increase in fluctuations near the transition from $T < 0$ to $T > 0$. This shows up as a slight increase in variance before it decreases. This effect is due to stochastic runs randomly getting "stuck" in the $T > 0$ regime when the equilibrium state is still $T < 0$, analogous to flickering between the two states of a double potential well, thereby increasing the variance.

In the simpler model (3), we take the annual mean global mean incident shortwave radiation from WE15, $S = 340\ \mathrm{W\ m^{-2}}$, and we use the equatorial ice-free coalbedo, $a = 0.7$. We set σ_1 to a value 20 times larger than in the full model (1). F is decreased from 15 to $-15\ \mathrm{W\ m^{-2}}$ over 1000 years. We use an integration time step of $\Delta t = 0.01$ year, and we use a sampling period of 1 year to compute σ^2 and ρ, as for model (2).

Acknowledgments
We thank John Wettlaufer, Sebastian Bathiany, Dirk Notz, Vasilis Dakos, and Peter Ditlevsen for their helpful comments on an earlier version of this paper. This work was supported by ONR grant N00014-13-1-0469. Code to numerically solve the model described in (1) is available at http://eisenman.ucsd.edu/code.html.

References

Boettiger, C., and A. Hastings (2012a), Early warning signals and the prosecutor's fallacy, *Proc. R. Soc. B*, *279*(1748), 4734–4739.
Boettiger, C., and A. Hastings (2012b), Quantifying limits to detection of early warning for critical transitions, *J. R. Soc. Interface*, *9*(75), 2527–2539.
Boettiger, C., and A. Hastings (2013), No early warning signals for stochastic transitions: Insights from large deviation theory, *Proc. R. Soc. B*, *280*(1766), 20131372.
Boulton, C. A., and T. M. Lenton (2015), Slowing down of North Pacific climate variability and its implications for abrupt ecosystem change, *Proc. Natl. Acad. Sci. U.S.A.*, *112*(37), 11,496–11,501.
Carpenter, S. R., and W. A. Brock (2006), Rising variance: A leading indicator of ecological transition, *Ecol. Lett.*, *9*(3), 308–315.
Dakos, V., M. Scheffer, E. H. van Nes, V. Brovkin, V. Petoukhov, and H. Held (2008), Slowing down as an early warning signal for abrupt climate change, *Proc. Natl. Acad. Sci. U.S.A.*, *105*(38), 14,308–14,312.
Dakos, V., E. H. van Nes, P. D'Odorico, and M. Scheffer (2012), Robustness of variance and autocorrelation as indicators of critical slowing down, *Ecology*, *93*(2), 264–271.
Dakos, V., S. R. Carpenter, E. H. van Nes, and M. Scheffer (2015), Resilience indicators: Prospects and limitations for early warnings of regime shifts, *Proc. R. Soc. B*, *370*(1659), 20130263.
Ditlevsen, P. D., and S. J. Johnsen (2010), Tipping points: Early warning and wishful thinking, *Geophys. Res. Lett.*, *37*, L19703, doi:10.1029/2010GL044486.
Eisenman, I. (2012), Factors controlling the bifurcation structure of sea ice retreat, *J. Geophys. Res.*, *117*, D01111, doi:10.1029/2011JD016164.
Eisenman, I., and J. S. Wettlaufer (2009), Nonlinear threshold behavior during the loss of Arctic sea ice, *Proc. Natl. Acad. Sci. U.S.A.*, *106*(1), 28–32.
Goosse, H., O. Arzel, C. M. Bitz, A. de Montety, and M. Vancoppenolle (2009), Increased variability of the Arctic summer ice extent in a warmer climate, *Geophys. Res. Lett.*, *36*, L23702, doi:10.1029/2009GL040546.
Hasselmann, K. (1976), Stochastic climate models. Part I. Theory, *Tellus A*, *28*, 473–485.
Held, H., and T. Kleinen (2004), Detection of climate system bifurcations by degenerate fingerprinting, *Geophys. Res. Lett.*, *31*, L23207, doi:10.1029/2004GL020972.
Hong, H., and J. C. Stein (2003), Differences of opinion, short-sales constraints, and market crashes, *Rev. Financ. Stud.*, *16*(2), 487–525.
Kefi, S., V. Dakos, M. Scheffer, E. H. van Nes, and M. Rietkerk (2013), Early warning signals also precede non-catastrophic transitions, *Oikos*, *122*(5), 641–648.
Kleinen, T., H. Held, and G. Petschel-Held (2003), The potential role of spectral properties in detecting thresholds in the Earth system: Application to the thermohaline circulation, *Ocean Dyn.*, *53*(2), 53–63.
LeBaron, B. (1992), Some relations between volatility and serial correlations in stock market returns on JSTOR, *J. Bus.*, *59*, 199–219.
Lenton, T. M. (2012), Arctic climate tipping points, *Ambio*, *41*(1), 10–22.
Lenton, T. M., H. Held, E. Kriegler, J. W. Hall, W. Lucht, S. Rahmstorf, and H. J. Schellnhuber (2008), Tipping elements in the Earth's climate system, *Proc. Natl. Acad. Sci. U. S. A.*, *105*(6), 1786–1793.
Lenton, T. M., V. N. Livina, V. Dakos, E. H. van Nes, and M. Scheffer (2012), Early warning of climate tipping points from critical slowing down: Comparing methods to improve robustness, *Proc. R. Soc. A*, *370*(1962), 1185–1204.
Livina, V. N., and T. M. Lenton (2013), A recent tipping point in the Arctic sea-ice cover: Abrupt and persistent increase in the seasonal cycle since 2007, *Cryosphere*, *7*(1), 275–286.
Moon, W., and J. S. Wettlaufer (2011), A low-order theory of Arctic sea ice stability, *Europhys. Lett.*, *96*(3), 39001.
Notz, D. (2009), The future of ice sheets and sea ice: Between reversible retreat and unstoppable loss, *Proc. Natl. Acad. Sci. U. S. A.*, *106*(49), 20,590–20,595.
Pierrehumbert, R. T., D. S. Abbot, A. Voigt, and D. Koll (2011), Climate of the neoproterozoic, *Annu. Rev. Earth Planet. Sci.*, *39*(1), 417–460.
Scheffer, M., J. Bascompte, W. A. Brock, V. Brovkin, S. R. Carpenter, V. Dakos, H. Held, E. H. van Nes, M. Rietkerk, and G. Sugihara (2009), Early-warning signals for critical transitions, *Nature*, *461*(7260), 53–59.
Scheffer, M., et al. (2012), Anticipating critical transitions, *Science*, *338*(6105), 344–348.
Wagner, T. J. W., and I. Eisenman (2015), How climate model complexity influences sea ice stability, *J. Clim.*, *28*(10), 3998–4014.
Walsh, J. E., I. Shapiro, and T. L. Shy (2005), On the variability and predictability of daily temperatures in the Arctic, *Atmos. Ocean*, *43*(3), 213–230.
Winton, M. (2006), Does the Arctic sea ice have a tipping point?, *Geophys. Res. Lett.*, *33*, L23504, doi:10.1029/2006GL028017.
Wissel, C. (1984), A universal law of the characteristic return time near thresholds, *Oecologia*, *65*(1), 101–107.